Directivity models produced for the Next Generation Attenuation West 2 (NGA-West 2) project

Paul Spudich
U.S. Geological Survey, Menlo Park CA, USA

Jennie Watson-Lamprey
Watson-Lamprey Consulting, Berkeley CA, USA

Paul Somerville and Jeff Bayless
URS Corporation, CA, USA

Shrey Shahi and Jack W. Baker
Stanford University, Stanford, CA, USA

Badie Rowshandel
California Earthquake Authority, Sacramento CA, USA

Brian Chiou
California Department of Transportation, Sacramento, CA, USA

SUMMARY
Five new directivity models are being developed for the NGA-West 2 project. All are based on the NGA-West 2 data base, which is considerably expanded from the original NGA-West data base, containing about 3,000 more records from earthquakes having finite-fault rupture models. All of the new directivity models have parameters based on fault dimension in km, not normalized fault dimension. This feature removes a peculiarity of previous models which made them inappropriate for modeling large magnitude events on long strike-slip faults. Two models are explicitly, and one is implicitly, 'narrowband' models, in which the effect of directivity does not monotonically increase with spectral period but instead peaks at a specific period that is a function of earthquake magnitude. These narrowband models' functional forms are capable of simulating directivity over a wider range of earthquake magnitude than previous models. The functional forms of the five models are presented.

Keywords: Ground motion prediction models, attenuation, directivity

1. INTRODUCTION

This report summarizes the improved seismic directivity models which are being developed as part of the NGA-West 2 project (http://peer.berkeley.edu/ngawest2/) by five teams comprised of subsets of the authors of this report. The five teams (with name abbreviations to be used henceforth) are: 1) J. Baker and S. Shahi (BS), who are adapting the Shahi and Baker (2011) pulse probability model, 2) B. Rowshandel (R), who is revising the Rowshandel (2010) directivity model, 3) P. Somerville and J. Bayless (SB), who are revising the classic Somerville et al. (1997) model, 4) P. Spudich and B. Chiou (SC), who are revising the Spudich and Chiou (2008) model, and 5) J. Watson-Lamprey (WL), who is presenting a new model. Of the five teams, two teams' (R, SC) earlier models were developed based on the original database of the Next Generation Attenuation West (NGA-West, http://peer.berkeley.edu/ngawest/index.html) project (Chiou et al., 2008).

A shortcoming of the NGA-West project, vis-a-vis directivity, was that the directivity models were developed as after-the-fact corrections to be added to the five ground-motion prediction equations (GMPEs) produced by the NGA-West project (Abrahamson and Silva, 2008; Boore and Atkinson, 2008; Campbell and Bozorgnia, 2008; Chiou and Youngs, 2008; and Idriss, 2008; abbreviated AS, BA, CB, CY, and ID, respectively). This was problematic for three reasons. First, since the original NGA-West data had directivity amplifications or deamplifications in them, these directivity signals

were probably fit to some extent by other inappropriate non-directive terms (e.g. the hanging wall amplification) in the developed GMPEs. Consequently, models like Rowshandel (2010) and Spudich and Chiou (2008) probably underestimate the actual amount of directivity in the data. Second, the NGA-West data set was probably biased in terms of directivity. In other words, the average directivity value of the whole data set was not zero. (For example, imagine that the entire NGA-West data set consisted of the four local recordings of the 1966 Parkfield earthquake, all of which were in a forward-directivity zone. GMPEs fit to these data would fit them using magnitude and distance-dependent terms, leaving small residuals that would imply small directivity.) Third, most of the NGA-West GMPE developers smoothed their coefficients as a function of spectral period, deliberately degrading the data fits at some frequencies, and they left in a mean bias with respect to distance. Post-hoc fitting of directivity to the GMPE residuals had the effect of unsmoothing the directivity-corrected GMPEs and removing the deliberate distance bias.

The two main goals of the directivity modelers are 1) to improve the models based on the expanded NGA-West 2 data set, and 2) to produce directivity models that can be included as additional terms in the development of new NGA-West 2 GMPEs, with the directivity coefficients being determined in the same regression as the other GMPE coefficients. The new NGA-West 2 GMPE developer teams are the same as the NGA-West teams.

2. DATA

The NGA-West data set had 3,551 three-component accelerograms, and the NGA-West 2 project has 8,661 three-component accelerograms. However, only records from earthquakes having finite-fault rupture models were usable to study directivity. An ad-hoc working group of the NGA-West 2 project selected finite-fault models by reviewing the literature to find rupture models produced for each earthquake by wave-form modeling. Each earthquake's source model was then parameterized the same way that the NGA sources were parameterized (Chiou et al. 2008). Table 1 lists the earthquakes with finite-fault models in the NGA-West 2 data set not present in the NGA data set. Also listed are the total number of three-component records, the number of records recorded at sites having Joyner-Boore distances (Rjb) less than or equal to 50 and 5 km, and the minimum and maximum Rjb for all sites. Fig. 2.1 shows the NGA (red plus signs) and the new NGA-West 2 (blue circles) finite-fault data sets' distributions in magnitude and rupture distance Rrup, for $0 < Rrup < 50$ km, the distance range important for near-fault directivity. The new data do not add many records at $Rjb < 5$ km except for the 2004 Parkfield, California, earthquake, which was anticipated to occur on a specific, well-defined section of the San Andreas fault, so many accelerographs were pre-positioned close to the fault trace (Shakal et al., 2005).

The directivity model development plan called for two stages. In the first stage the directivity modeling teams were to develop functional forms for their new models based on the NGA-West 2 data set, and optionally, develop approximate coefficients appropriate for each NGA or preliminary NGA-West 2 GMPE available at the time. These functional forms and coefficients were to be submitted to the GMPE developers, who, in the second stage would include the directivity functional forms in their GMPE development. Data for the first stage of the new directivity model development were produced as follows. GMPE developer teams AS and CB had derived interim improvements on their 2008 models, and gave the directivity modelers total pseudo-spectral acceleration (PSA) residuals from their interim models for all used NGA-West 2 records. GMPE developer teams BA, CY, and ID provided their list of selected NGA-West 2 records, and we calculated total residuals from their 2008 GMPEs applied to the NGA-West 2 data set. Using a mixed-effect model, we then fit a constant to each GMPE developer's set of residuals for only the earthquakes having finite-fault models. The resulting intra-event residuals from the mixed-effect fitting were used as data for the first stage of directivity model development.

Table 1: Earthquakes with finite-fault rupture models in the NGA-West 2 data set but not in the NGA-West data set.

Earthquake name	Year	Mo/da	Hr:mn	M	# recs	min Rjb	max Rjb	#Rjb <= 50km	#Rjb <= 5km
Joshua Tree, Calif.	1992	04/23	04:50	6.10	5	17.1	29.0	5	0
Tottori, Japan	2000	10/06	04:30	6.61	414	0.8	333.2	34	1
San Simeon, Calif.	2003	12/22	19:15	6.52	68	5.1	524.3	7	0
Bam, Iran	2003	12/26	01:56	6.60	24	0.1	282.2	3	1
Parkfield, Calif.	2004	09/28	17:15	6.00	141	0.0	373.8	75	41
Niigata, Japan	2004	10/23	08:56	6.63	530	0.2	297.1	31	4
Montenegro, Yugoslavia	1979	04/15	06:19	7.10	11	0.0	118.2	5	4
L'Aquila, Italy	2009	04/06	01:33	6.30	48	0.0	227.1	19	5
Wenchuan, China	2008	05/12		7.90	263	0.0	1532.7	19	6
Chuetsu-oki, Japan	2007	07/16	10:13	6.80	616	0.0	299.9	85	15
Iwate, Japan	2008	06/13	23:43	6.90	67	0.0	279.4	80	2
El Mayor-Cucapah, Mexico	2010	04/04	22:40	7.20	361	8.9	620.8	26	0
Darfield, New Zealand	2010	09/03	16:35	7.00	114	0.0	540.9	34	2
Christchurch, New Zealand	2011	02/21	23:51	6.10	104	0.0	444.9	27	7

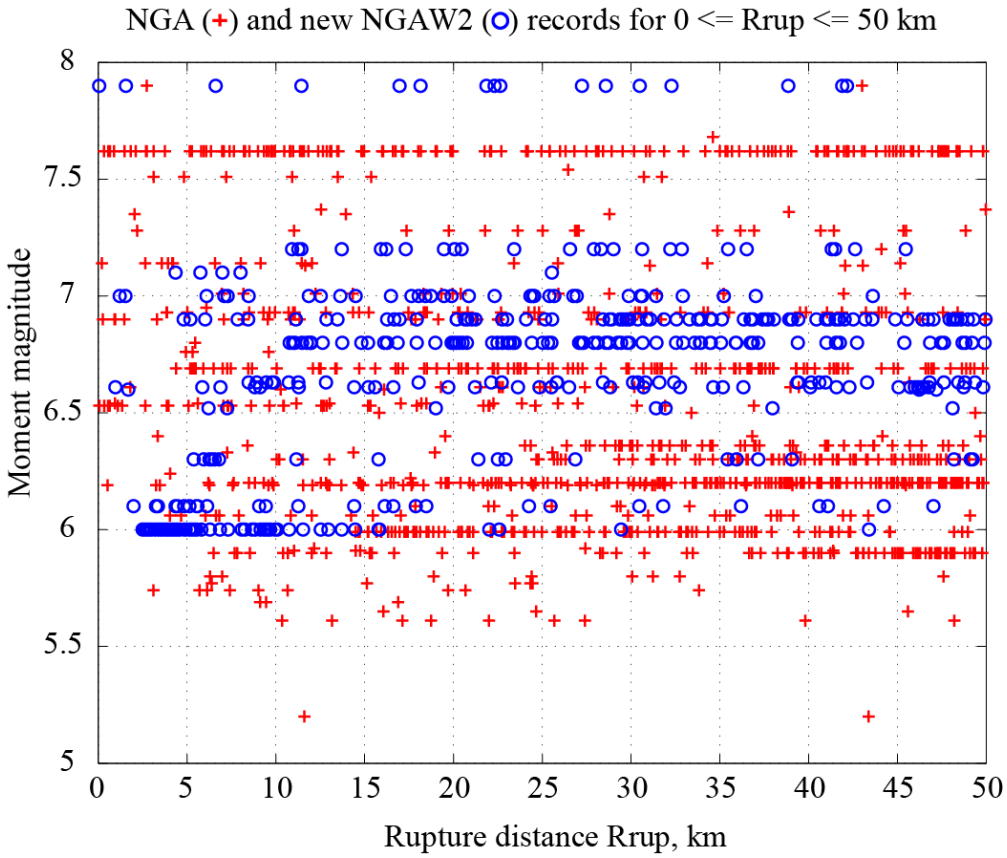

Figure 2.1: Distribution of data from shallow crustal earthquakes having finite-fault models. Red plus (+) signs are from the NGA-West data base; blue circles are additional records in the NGA-West 2 data base.

3. CONCEPTUAL ADVANCES

3.1 Unnormalized fault dimensions

The directivity parameters in all the new NGA-West 2 directivity models are functions of unnormalized fault dimensions (e.g. length in km) in order to avoid the following problem. Directivity models which are posed in terms of normalized fault dimensions, like the classic Somerville et al. (1997) and like Rowshandel (2010), have a flaw illustrated in Fig. 3.1. That figure compares the Somerville et al. (1997) directivity parameter $X \cos\theta$ for two vertical strike-slip earthquakes, a 300-km-long M7.8 and a 150-km-long M7.5, both evaluated at a site on strike 150 km from the epicenter. Both of these sites are equidistant from the epicenter and have the same length of fault rupturing toward them. This implies that they should experience a similar directivity effect. However, Somerville's directivity model predicts a directivity parameter of 0.5 at site 1 and 1.0 at site 2, i.e. it predicts twice the directivity at site 2 compared to site 1. This flaw limits the use of these relations for large magnitude earthquakes on long strike-slip faults. Abrahamson (2000) circumvented this problem by capping $X \cos\theta$ for long ruptures, and Spudich and Chiou (2008) and Shahi and Baker (2011) used unnormalized fault dimensions.

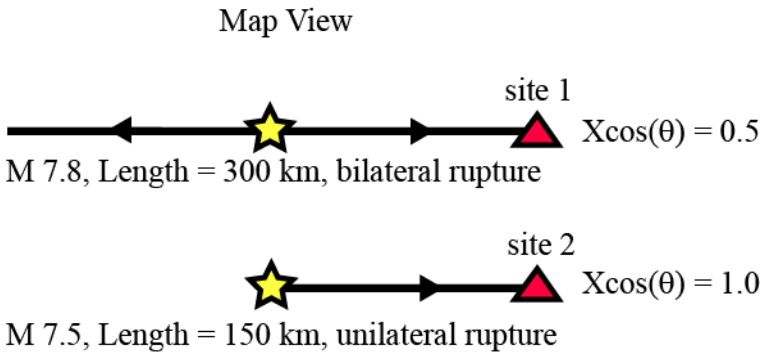

Figure 3.1: Schematic map of two vertical strike slip ruptures. Stars are epicenters, triangles are sites, arrows show direction of rupture propagation. For the M 7.8, rupture of the 150 km right limb gives a directivity factor of 0.5 at site 1, whereas the rupture of 150 km of the M 7.5 yields a directivity factor of 1.0 at site 2.

3.2 Narrowband directivity models

Three of the NGA-West 2 directivity models are so-called 'narrowband' directivity models, in which the spectral period of peak directivity amplification varies as a function of magnitude. Two curious features of many older directivity models, such as Somerville et al. (1997), Abrahamson (2000), and Spudich and Chiou (2008) are that 1) all earthquakes have their peak directivity at the longest spectral periods, regardless of magnitude, and 2) earthquakes having magnitudes less than about 6.0 have very little or no directivity. Seekins and Boatwright (2010) have shown that many earthquakes of M 3.5 - 5.4 have clear directivity in their PGA and PGV, so the lack of directivity for small earthquakes in these older directivity models points to a flaw in the functional forms. Baker (2007) has shown that the presence of a directivity pulse in a record causes a peak in the spectral velocity near the period of the pulse, and it causes the long period corner of the PSA to be near the pulse period. The new BS and SC models implement a narrowband model explicitly. Fig. 3.2 shows how the period of the peak directivity in the BS model varies as a function of magnitude. The SC model shows a similar behavior with somewhat wider peaks (not shown). The WL model is not explicitly narrowband, but has some narrowband characteristics as described below.

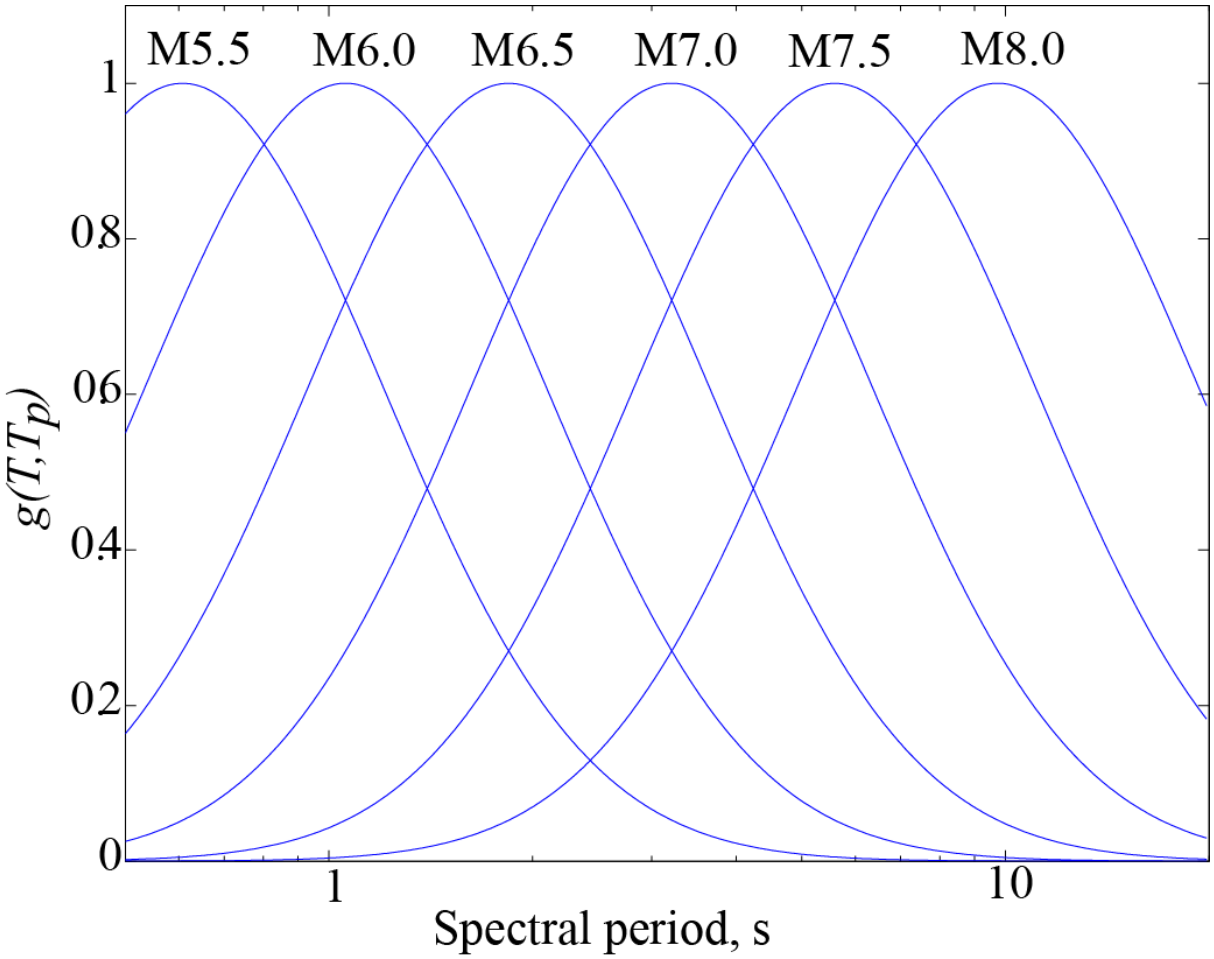

Figure 3.2: Illustration of broadband behavior of BS directivity model. Period of peak directivity shifts to long period for larger magnitudes, indicated above related peak.

4. A BRIEF SUMMARY OF THE NGA-WEST 2 DIRECTIVITY MODELS

At the time of this writing, the functional forms of the new directivity models have been largely developed, but they have not had their coefficients determined in a regression by the GMPE developers. Consequently, we review each model but omit specific values of coefficients.

4.1 Baker and Shahi model (BS)

Unlike the other directivity models, the BS model simulates the probability of occurrence and the characteristics of a directivity pulse at a site. The new model is based on the formalism of Shahi and Baker (2011) with coefficients to be derived from the NGA-West 2 data set. Briefly, if a standard GMPE is of the form

$$\boldsymbol{ln\ PSA = f(M,R,T,\ldots) + \phi\varepsilon + \tau\eta} \tag{4.1}$$

where $\boldsymbol{M}$ is moment magnitude, $\boldsymbol{T}$ is spectral period, $\boldsymbol{R}$ is distance (typically rupture distance), $\boldsymbol{\varepsilon}$ is a Gaussian random variable with zero mean and standard deviation $\boldsymbol{\phi}$ associated with each record, and $\boldsymbol{\eta}$ is a Gaussian random variable with zero mean and standard deviation $\boldsymbol{\tau}$ associated with each earthquake, then the modified GMPE is

$$\boldsymbol{ln\ PSA = f(M,R,T,\ldots) + I_{Pulse}\ g(T,T_p) + \phi\varepsilon + \tau\eta} \tag{4.2}$$

where

$$g(T, T_p) = b_o exp\left[-b_1 (ln(T/T_P) + b_2)^2\right] \quad (4.3)$$

$$P(I_{Pulse} = 1) = 1/[1 + exp(c_1 + c_2 r + c_3 s + c_4 \theta)] \quad (4.4)$$

$$ln\, T_P = c_5 + c_6 M. \quad (4.5)$$

Note that the coefficients are independent of period, so that the regression of the ground motion data is done for all periods in a single step. Geometric parameters r, s, and θ are defined in Shahi and Baker (2011).

4.2 B. Rowshandel model (R)

This model has three major changes compared to Rowshandel (2010). First, in previous work Rowshandel's directivity parameter ξ was based on only the angle between a unit vector in the rupture direction ($\vec{p}$ in Fig. 4.1) and a unit vector in the direction to the site ($\vec{q}$ in Fig. 4.1). In his new relation, the directivity parameter is proportional to $(\vec{q} \cdot \vec{s} + \vec{q} \cdot \vec{p})/2$, where $\vec{s}$ is a unit vector in the direction of slip (see Fig. 4.1). Second, to unnormalize his directivity parameter (see section 3.1) Rowshandel has replaced ξ with $\xi' = \xi\, ln(L_r)/ln(L_{rmax})$, where L_r is the 'effective rupture length', and L_{rmax} is L_r for $M = M_{max}$ ($L_{rmax} \cong 400$ km for $M_{max} = 8.5$). The third change is to prohibit negative values of ξ', such as would have occurred for the geometry of Fig. 4.1. To apply this directivity model to a GMPE, the directivity parameter ξ', multiplied by a period-dependent empirical directivity coefficient C, is added to the GMPE.

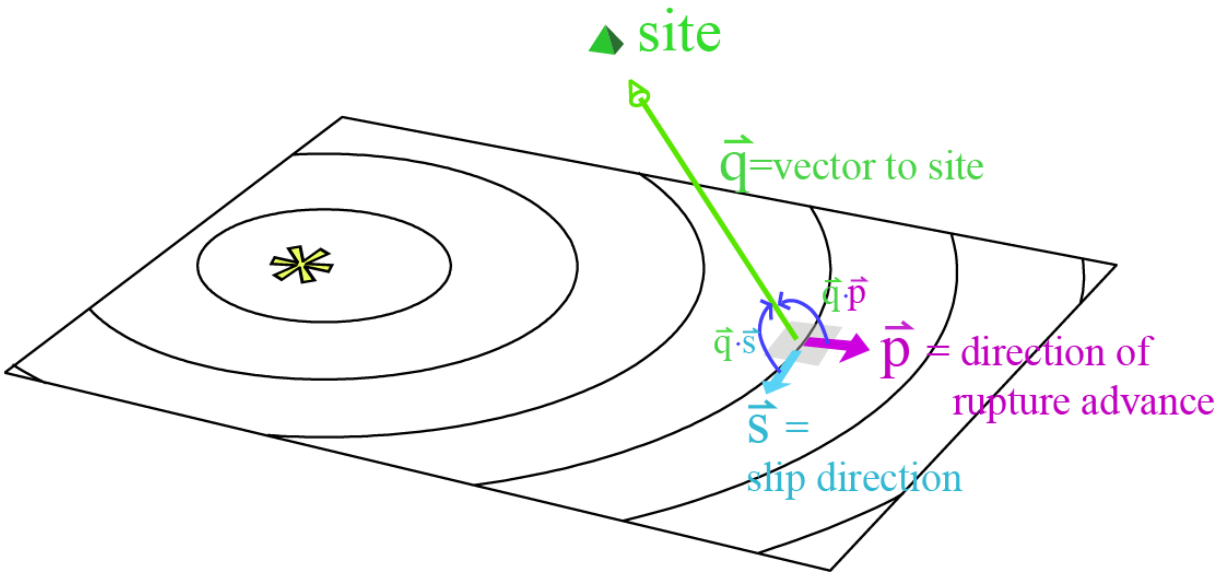

Figure 4.1: Angles used in new R directivity model. Yellow asterisk is earthquake hypocenter, rectangle is the fault surface (seen in perspective), ellipses are rupture position (seen in perspective) at various times. The direction of the slip unit vector is not in general perpendicular to the direction of rupture advance, but is drawn that way to make clear the angles between the vectors. Similarly, for the illustrated site location, both the qp and qs angles are greater than 90° for illustrative purposes, but for that reason the subfault shown does not contribute to directivity at the site.

4.3 Somerville and Bayless (SB)

SB's new relation is similar in its simplicity to the classic Somerville et al. (1997) relation, but they have unnormalized it with respect to fault length. It has the form

$$\boldsymbol{ln\ PSA = f(M,R,T,\ldots) + \left(c_o + c_1 f_{geom}\right) \times}$$

$$\boldsymbol{\left(M, R_{rup}, Azimuth\ tapers\right) + \phi\varepsilon + \tau\eta} \tag{4.6}$$

where for strike-slip

$$\boldsymbol{f_{geom}(s,\theta) = ln(s)\ (0.5cos(2\theta) + 0.5)} \tag{4.7}$$

and for dip-slip

$$\boldsymbol{f_{geom}(d,R_x) = ln(d)\ \cos\ (R_x/W)} \tag{4.8}$$

and where $\boldsymbol{c_o}$ and $\boldsymbol{c_1}$ are period-dependent constants, $\boldsymbol{s}$ is the unnormalized length (in km) along the fault trace from the epicenter to the closest point on the fault trace to the site, $\boldsymbol{d}$ is the unnormalized width (in km) of the fault trace rupturing toward the site, $\boldsymbol{\theta}$ is the same as in Somerville et al. (1997), $\boldsymbol{R_x}$ is the horizontal distance (in km) to the site from the top edge of rupture, and $\boldsymbol{W}$ is the total fault width (in km). The applicable ranges of the SB directivity parameters are as follows:

$$\boldsymbol{s \in [\exp(1), \infty],} \qquad \boldsymbol{d \in [1, \infty],} \qquad \boldsymbol{\theta \in [0, \frac{\pi}{2}],} \qquad \boldsymbol{R_x/W \in [-\frac{\pi}{2}, \frac{2\pi}{3}]} \tag{4.9}$$

4.4 Spudich and Chiou (SC)

SC have gone to a narrow-band directivity model of the form

$$\boldsymbol{ln\ PSA = f(M,R,T,\ldots) + \left(M, R_{rup}\ tapers\right) b(M,T)(IDP - a) + \phi\varepsilon + \tau\eta} \tag{4.10}$$

where

$$\boldsymbol{b(M,T)\ = \left(c_2 + c_3\ max(M - c_1, 0)\right) \times}$$

$$\boldsymbol{exp\left[-\left(log_{10}T\ -\ (c_4 + c_5 M)\right)^2 / 2s^2\ \right]} \tag{4.11}$$

where the ***IDP*** is defined in Spudich and Chiou (2008), *a* is a previously tabulated average value of the ***IDP*** for ruptures of magnitude ***M*** and the desired mechanism, $\boldsymbol{c_1}$... $\boldsymbol{c_5}$ and $\boldsymbol{s}$ are spectral-period-independent coefficients estimated by joint regression of combined data from all spectral periods.

4.5 Watson-Lamprey (WL)

WL's directivity parameter $\boldsymbol{Z}$, illustrated in Figure 4.2, is the integral of angle Θ along the line from the hypocenter to point D, where Θ = 45°. She has obtained an analytic expression for this integral, not presented here. The logic behind $\boldsymbol{Z}$ is that most of the directivity amplification comes from the SH pulse, for which the radiation pattern (as seen at the site) is largest when rupture is near the hypocenter. The form of the resulting modification term $\boldsymbol{f_D}$ added to the GMPE is

$$\boldsymbol{Z < 4T: f_D = 0,} \qquad \boldsymbol{Z > 60: f_D = b_7} \tag{4.12}$$

else

$$\boldsymbol{f_D = b_7\left(\left(lnZ - ln(4T)\right)/\left(ln60 - ln(4T)\right)\right).} \tag{4.13}$$

$\boldsymbol{b_7}$ is a period-dependent constant. WL's $\boldsymbol{Z}$ is not normalized to fault dimension. This model has some narrowband characteristics. The minimum $\boldsymbol{Z}$ value that has to be achieved in order to experience a directivity effect is $\boldsymbol{4T}$. So, for a M6 earthquake where $\boldsymbol{Z}$ is approximately 10, a directivity effect would be seen at $\boldsymbol{T}$ = 1 s but not for $\boldsymbol{T}$ > 2.5 s.

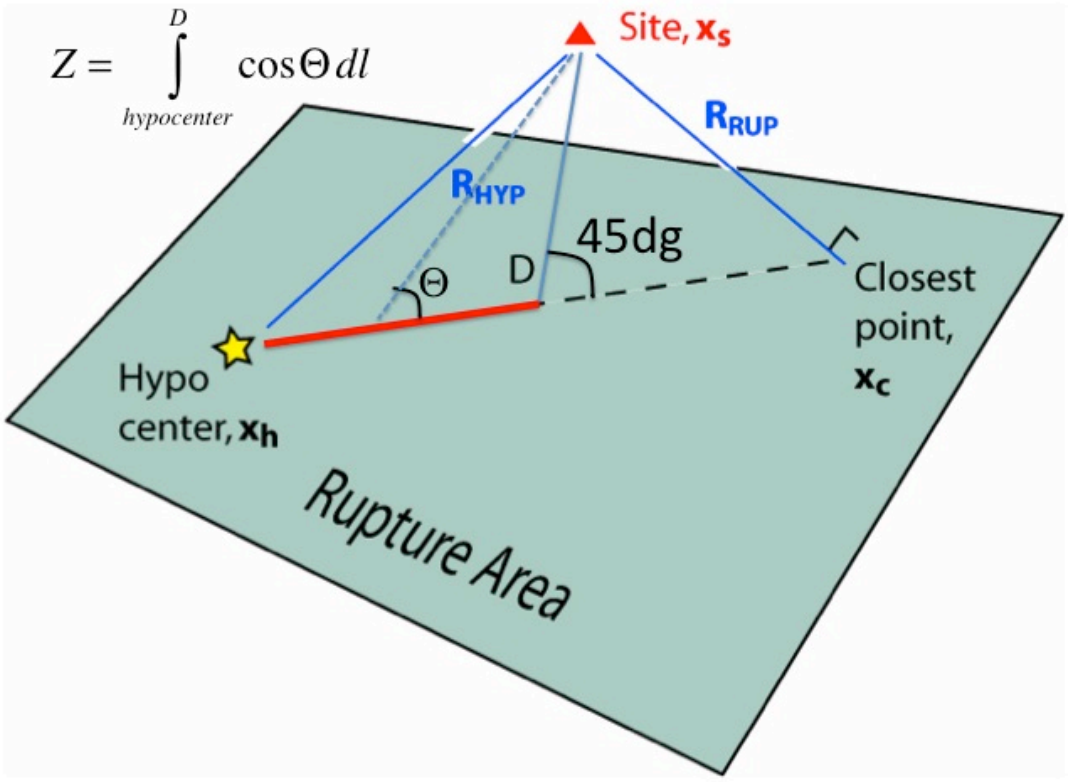

Figure 4.2: Illustration of WL geometry and directivity parameter. Point D is located on a line connecting the hypocenter to the closest point to the site. At D, the angle Θ is 45°.

ACKNOWLEDGEMENT

This study was sponsored by the Pacific Earthquake Engineering Research Center (PEER) and funded by the California Earthquake Authority, the California Department of Transportation, and the Pacific Gas & Electric Company. Any opinions, findings, and conclusions or recommendations expressed in this material are those of the authors and do not necessarily reflect those of the sponsoring agencies.

REFERENCES

Abrahamson, N. A. (2000). "Effects of rupture directivity on probabilistic seismic hazard analysis." *Sixth International Conference on Seismic Zonation*, Earthquake Engineering Research Inst., Oakland, California.

Abrahamson, N. (2000). Effects of rupture directivity on probabilistic seismic hazard analysis, *6th Int. Conf. on Seismic Zonation*, **Proceedings**: Earthq. Eng. Res. Inst. CD-2000-01.

Abrahamson, N., and Silva, W. (2008). Summary of the Abrahamson & Silva NGA ground motion relation. *Earthquake Spectra*. **24:1**, 67-97.

Baker, J. (2007). Quantitative classification of near-fault ground motions using wavelet analysis. *Bull. Seismol. Soc. Am*. **97:5**, 1486-1501.

Boore, D.M. and Atkinson, G.M. (2008). Ground-motion prediction equations for the average horizontal component of PGA, PGV, and 5%-damped PSA at periods between 0.01 s and 10.0 s. *Earthquake Spectra*. **24:1**, 99-138.

Campbell, K.W. and Bozorgnia, Y. (2008). NGA ground motion model for the geometric mean horizontal component of PGA, PGV, PGD, and 5%-damped linear elastic response spectra for periods ranging from 0.01 to 10 s. *Earthquake Spectra*. **24:1**, 139-171.

Chiou,B., Darragh, R., Gregor, N., and Silva, W. (2008). NGA project strong-motion database. *Earthquake Spectra,* **24:1**, 23-44.

Chiou, B.S.-J., and Youngs, R.R. (2008). An NGA model for the average horizontal component of peak ground motion and response spectra. *Earthquake Spectra,* **24:1**, 173-215.

Idriss, I.M. (2008). An NGA empirical model for estimating the horizontal spectral values generated by shallow crustal earthquakes. *Earthquake Spectra,* **24:1**, 217-242.

Rowshandel, B. (2010). Directivity correction for the next generation attenuation (NGA) relations, *Earthquake Spectra,* **26:2**, 525-559.

Seekins, L. and Boatwright, J. (2010). Rupture directivity of moderate earthquakes in northern California. *Bull. Seismol. Soc. Am.* **100:3, 1**107-1119.

Shahi, S. and Baker, J. (2011). An empirically calibrated framework for including the effects of near-fault directivity in probabilistic seismic hazard analysis. *Bull. Seismol. Soc. Am.* **101:2, 74**2–755.

Shakal, A., Graizer, V., Huang, M., Borcherdt, R., Haddadi, H., Lin, K-W., Stephens, C., and Roffers, P. (2005). Preliminary analysis of strong-motion recordings from the 28 September 2004 Parkfield, California earthquake.

Somerville, P.G., Smith, N.F., Graves, R.W., and Abrahamson, N.A. (1997). Modification of empirical strong ground motion attenuation relations to include the amplitude and duration effects of rupture directivity. *Seismol. Res. Let.* **68:1**, 199-222.

Spudich, P., and Chiou, B.S.-J. (2008). Directivity in NGA earthquake ground motions: Analysis using isochrone theory. *Earthquake Spectra,* **24:1**, 279-298.